J5J.2

Understanding the Generation of High Winds Associated with Bow Echoes: The Omaha Bow Echo during BAMEX

Roger M. Wakimoto[1], Hanne V. Murphey[1], David P. Jorgensen[2], Christopher A. Davis[3], and Nolan T. Atkins[4]

[1]Department of Atmospheric Sciences
UCLA
Los Angeles, CA 90095-1565

[2]NOAA/National Severe Storms Laboratory
Norman, OK 73069

[3]National Center for Atmospheric Research
Boulder, CO 80307

[4]Department of Meteorology
Lyndon State College
Lyndonville, VT 05851

1. Introduction

Fujita (1978) first documented the kinematic structure and time evolution of the radar echo of a mesoscale convective system (MCS) that he referred to as a bow echo. He showed that bow echoes were frequently associated with straight-line wind damage or downbursts at the surface. Although bow echoes have been known to produce damaging winds at the surface for a number of years, it is surprising that there is a relative dearth of detailed observational studies that have documented these events. In particular, there are no known comprehensive studies that have captured a significant portion of the life cycle of a bow echo. To the authors' knowledge, only Fujita (1981) has presented a multi-Doppler radar study of a severe bow echo while it produced destructive winds and a tornado; however, it was only for only analysis time and was confined to a single height.

The prevailing hypothesis for the generation of damaging winds at the surface has been the descent of the rear-inflow jet (e.g., Weisman 1993, and Przybylinski 1995). Extensive aerial and ground surveys in the aftermath of bow echoes have revealed large regions of destruction that could be attributed to a descending rear-inflow jet; however, there were pockets or swaths of more concentrated damage that occurred on a much smaller scale as shown by Forbes and Wakimoto (1983). Recently, Weisman and Trapp (2003) and Trapp and Weisman (2003) hypothesized, based on numerical simulations, that microburst damage was induced by strong low-level mesovortices. The intense low levels winds appeared to be accelerated by the large horizontal pressure gradients generated by these mesovortices.

A squall line developed over eastern Nebraska in the evening of 5 July 2003 during BAMEX (Bow echo and MCV Experiment; Davis et al. 2004). The radar echo associated with the line assumed a bow-shape near Omaha, NE during the time that numerous high wind reports were received by the NWS. Airborne radar measurements were made of the bow echo during the time is was creating damage rated F1 in intensity.

2. Storm movement and damage survey

An isochrone analysis of the radar reflectivity pattern associated with the storm during the period from 0200 to 0700 UTC (hereafter, all times are UTC) is shown in Fig. 1. The echo assumed a bow shape at ~0400. The echo maintained a convex shape for several hours until there was a rapid dissipation of the storm complex around 0700. Also plotted on Fig. 1 is the flight track of the NRL P-3 equipped with ELDORA.

The strong winds accompanying the bow echo led to widespread reports of damage in eastern Nebraska and western Iowa. Numerous tress were blow down and a number of structures were damaged. The result of detailed aerial and ground surveys over a 2.5-day period is presented in Fig. 2. The Omaha bow echo created an east-west

* *Corresponding author address*: Roger M. Wakimoto, NCAR/EOL, P.O. Box 3000, Boulder, CO 80307-3000; e-mail: wakimoto@ucar.edu

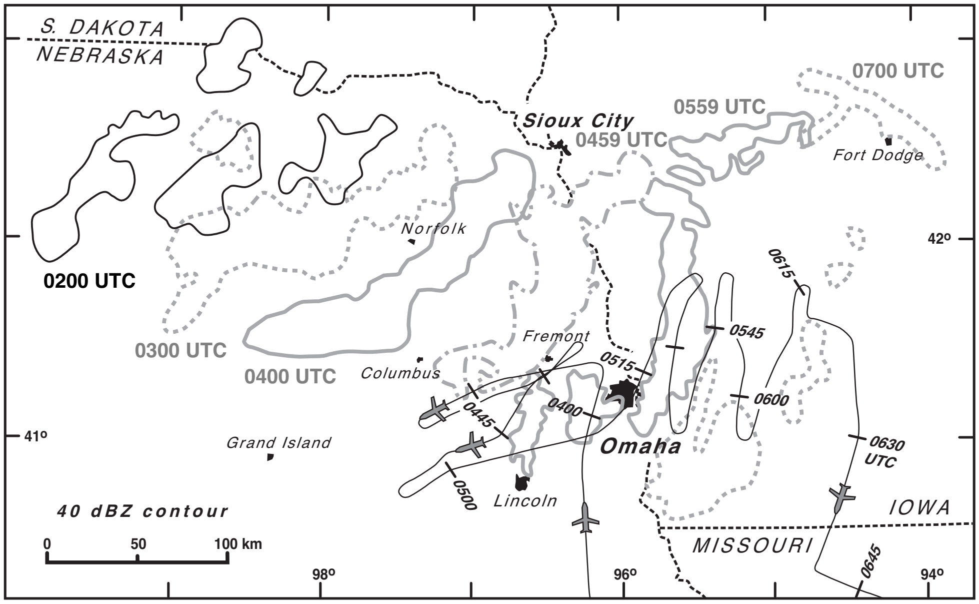

Fig. 1. Isochrone analysis of the Omaha bow echo. The 40 dBZ contour is drawn at 1-h intervals. The flight track of the NRL P-3 is shown.

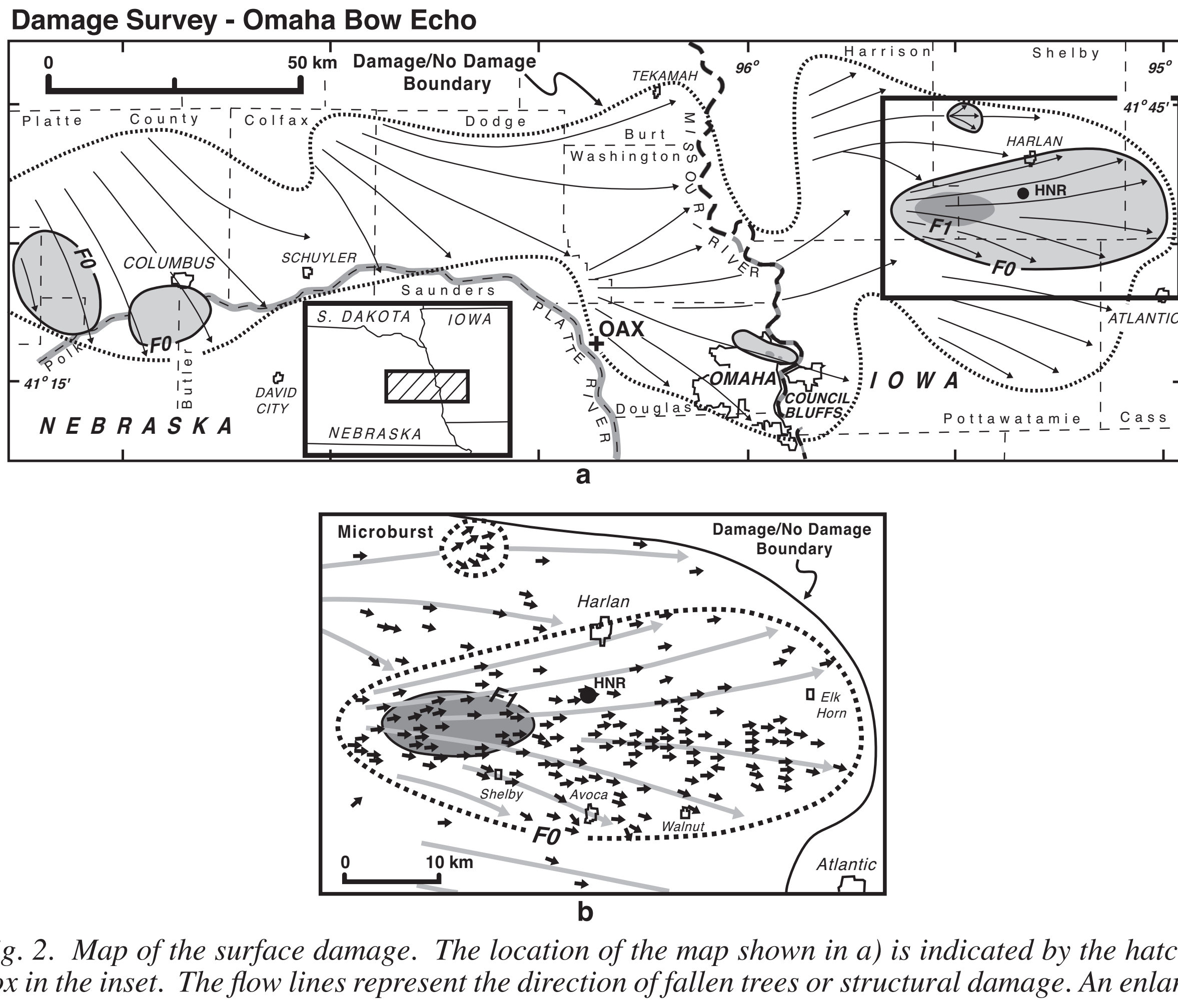

Fig. 2. Map of the surface damage. The location of the map shown in a) is indicated by the hatched box in the inset. The flow lines represent the direction of fallen trees or structural damage. An enlargement of the boxed-in region on the east side of a) is shown in b). The outer extent of the damage as well as the regions rated F0 and F1 in damage intensity are indicated in the figures.

swath of damage in eastern Nebraska and western Iowa that was ~50 km wide and 200 km long. The dotted line in Fig. 2 represents the region beyond which no damage was documented. There were several areas rated greater than F0 and one region of significant damage rated greater than F1 located ~20 km southwest of Harlan, Iowa.

An enlargement of the area experiencing the greatest damage in western Iowa is shown in Fig. 2b. The individual vectors of fallen trees/limbs and structural damage are shown. The classical depiction of a divergent wind pattern is apparent in the figure.

3. Doppler radar analyses

The Doppler radar data collected during the last five flight legs shown in Fig. 1 captured the entire evolution of the bowing process and are the focus of the present study. The third pass by the Omaha bow echo is shown in Fig. 3 and represents the time when the damage rated >F1 was occurring in western Iowa. There is a pronounced convex shape to the convective line as the apex of the bow echo surges to the east. A mesovortex, that was first detected during the early passes by the storm, is clearly evident in the vertical vorticity field at this time.

Vertical cross sections through the mesovortex during the previous two passes are shown in Fig. 4. The vertical cross section at 0510 - 0522 (Fig. 4a) shows that the strongest vertical vorticity is near the surface. The circulation tilts westward with increasing height but only extends a few kilometers above the surface. The quasi-linear convective line had begun to "bow out" dur-

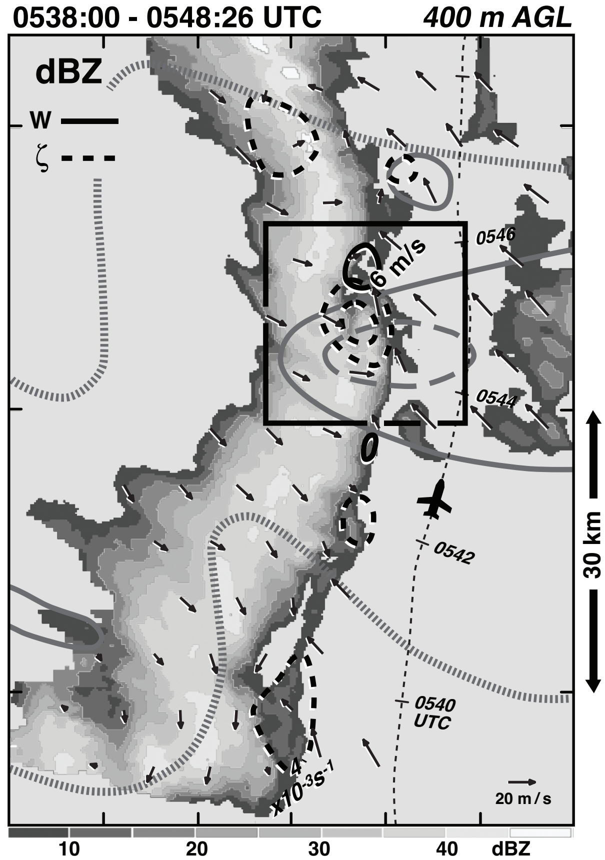

Fig. 3. Dual-Doppler wind synthesis at 0538:00 - 0548:26 UTC at 400 m AGL. Storm-relative winds are superposed onto radar reflectivity. Vertical vorticity (dashed lines) and vertical velocity (solid black lines) are plotted. The damage at the surface is based on the results in Fig. 2. The dotted gray, solid gray and dashed gray lines represent the damage/no damage boundary, F0 contour, and F1 contour, respectively.

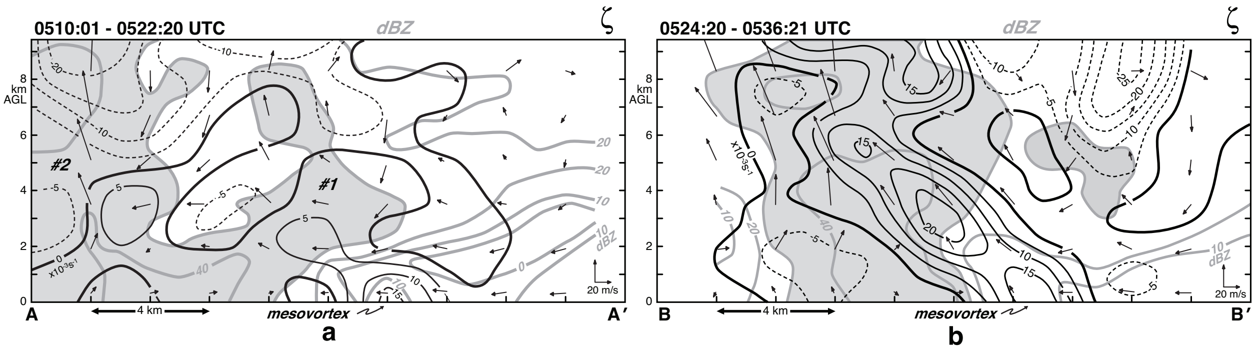

Fig. 4. West-East vertical cross sections through the mesovortex at a) 0510:01 - 0522:20 and b) 0524:20 - 0536:21 UTC. Gray lines are radar reflectivity. Black and dashed lines are positive and negative vertical vorticity values. The storm-relative winds in the plane of the cross section are plotted.

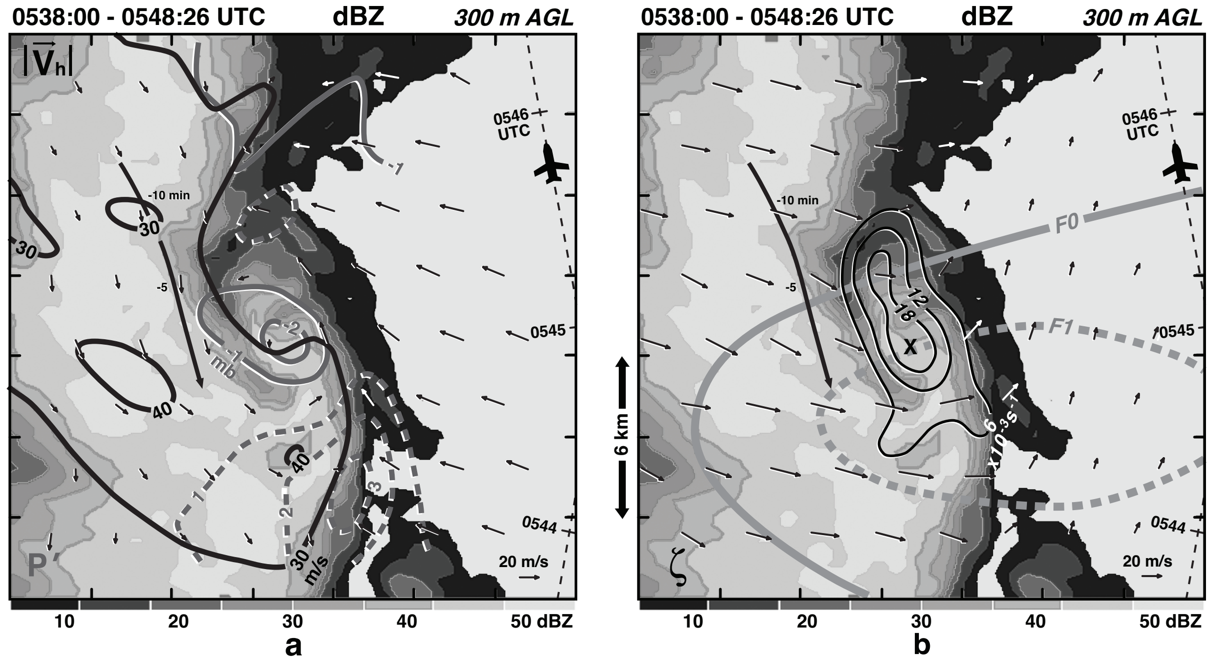

Fig. 5. Dual-Doppler wind syntheses at 0538:00 - 0548:26 UTC at 300 m AGL. Radar reflectivity is shown on both panels. a) Storm-relative winds, perturbation pressure (gray and dashed gray lines), and isotachs of horizontal velocity (black lines). b) Ground-relative winds, vertical vorticity (black lines), and F-scale analyses of the damage survey (gray and dashed gray lines). The trajectory of a parcel that is associated with the strongest winds at 300 m AGL is shown on both panels.

ing the second pass in response to an intensifying and descending rear-inflow jet. The mesovortex in Fig. 4b is embedded within an updraft and now appears to extend to 7-8 km AGL (hereafter, all heights are AGL). The intense outflow that has developed is evident by the pronounced tilt in the mesovortex with height.

A feature that resembles a hook echo has developed at the apex is collocated with the mesovortex (Fig. 3). This represents clear evidence that a relationship exists between the strongest surface damage and mesovortices.

An enlargement of the bow apex at 0538 - 0548 is shown in Fig. 5. The relationship between the mesovortex and the region of damage rated >F1 is shown (Fig. 5b). The hook echo noted in Fig. 3 is clearly evident and is approximately 9 km in diameter. The mesovortex has entered its most intense phase and a pronounced circulation can be identified in the storm-relative wind field. The mesovortex is not centered within the F1 contour but is displaced to the north. The 30 m s^{-1} isotach outlines a pronounced tongue of high wind speeds that is wrapping around the western and southern periphery of the mesovortex in Fig. 5a. Peak speeds > 40 m s^{-1} are close to the leading edge of the gust front and within the F1 contour.

4. The origin of strong surface winds

Trapp and Weisman (2003) hypothesize that the horizontal pressure gradients produced by the mesovortices in their simulations are important in creating regions of high speeds. In order to test this hypothesis, the perturbation pressure field was retrieved from the Doppler wind syntheses (Fig. 5a). The gust front, except at the location of the mesovortex, is characterized by a ridge of high perturbation pressure owing to the fluid extension term in the diagnostic pressure equation (i.e., strong horizontal convergence at the frontal boundary). The mesovortex was accompanied by a mesolow with a minimum pressure <-2 mb that was positioned near the tip of the hook echo.

Backward trajectories for a number of air parcels that terminated near the tip of the tongue of high wind speeds in Fig. 5a were calculated in order to isolate the possible forcing mechanisms. A representative trajectory is drawn in the figure.

A plot of the forces that create high winds along the trajectory (not shown) strongly suggest that the perturbation pressure gradient force is important in generating damaging wind speeds in bow echoes. This appears to substantiate the hypothesis advanced by Trapp and Weisman (2003).

A closer examination of the wind field, however, suggests that the pressure forces alone do not fully explain the observed pattern of high winds near the surface. The parcel trajectory would be expected to terminate closer to the center of the mesolow if the pressure gradients created by the circulation dominated. Instead, the parcel skirts around the periphery of the mesolow. Further evidence is the tongue-shaped structure of the 30 m s^{-1} isotach in Fig. 5 which wraps around the mesovortex and mesolow.

The displacement of the high wind speeds (and damage) to the southern flank of the mesovortex is reminiscent of the superposition of a vortex and the flow in which it is embedded. This type of asymmetry is commonly observed during post-storm surveys of tornado and hurricane damage. The strongest winds typically occur on the side of the vortex where translational and rotational effects are in the same direction.

An attempt was made to determine whether a vortex superposition onto the flow could explain the wind field shown in Fig. 5. The Poisson equation for the perturbation streamfunction $(\nabla^2 \psi' = \zeta)$ was solved assuming that the vertical vorticity was zero everywhere outside of the mesovortex and that the perturbation streamfunction was equal to zero on the lateral boundaries. The retrieved streamfunction was used to compute the non-divergent component of the wind field. These winds were subsequently subtracted from the Doppler wind syntheses to create a modified wind field without the effect of the mesovortex (Fig. 6).

The impact of the mesovortex is illustrated by comparing the two plots shown in the figure. The pocket of high winds (> 35 m s^{-1}) responsible for the F1 damage on the southern periphery of the mesovortex has been removed in Fig. 6b. The strongest postfrontal winds are now displaced much farther to the north and appear to be a result of the descending rear-inflow jet as would be expected.

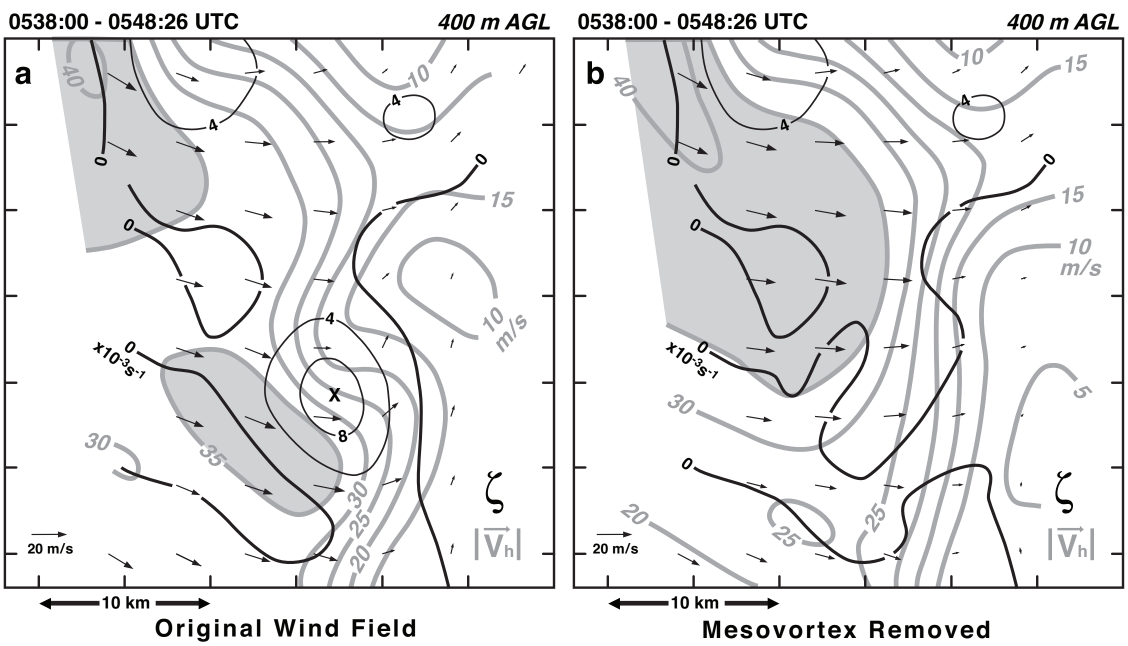

Fig. 6. Doppler wind syntheses at 0538:00 - 0548:26 UTC at 400 m AGL superimposed onto vertical vorticity, isotachs, and the ground-relative Doppler wind synthesis for a) the original analysis and b) with the circulation associated with the mesovortex removed. Black lines and vertical vorticity and isotachs, respectively. Areas shaded gray are > 35 m s^{-1}.

5. Summary and discussion

The entire evolution of a quasi-linear convective line that evolves into a bow-shaped echo was presented. The precise locations of the damaging surface winds was determined by a detailed aerial and ground survey. The regions of most intense, damaging straight-line winds were near mesovortices that developed along the gust front. The preferred regions of intense surface winds can best be described as a superposition of the vortex and the flow in which it is embedded.

This finding supports the damage survey presented by Forbes and Wakimoto (1983). Several tornadoes documented in their study were accompanied by microburst damage located immediately to the south of the tracks. The strongest winds would be expected at that location since it is the side where translation and rotation effects are in the same direction. A key question that remains unanswered is the relationship between intense mesovortices and bow-echo tornadoes. Unfortunately, no multi-Doppler data was collected on a tornado spawned by a bow echo during BAMEX.

Acknowledgements. Research results presented in this paper were supported by the National Science Foundation under Grants ATM-021048 (through RMW) and ATM-0233178 (through NTA).

References

Davis, C., N. Atkins, D. Bartels, L. Bosart, M. Coniglio, G. Bryan, W. Cotton, D. Dowell, B. Jewett, R. Johns, D. Jorgensen, J. Knievel, K. Knupp, W.-C. Lee, G. McFarquhar, J. Moore, R. Przybylinski, R. Rauber, B. Smull, R. Trapp, S. Trier, R. Wakimoto, M. Weisman and C. Ziegler. 2004: The Bow echo and MCV Experiment: Observations and opportunities. *Bull. Amer. Meteor. Soc.*, **85**, 1075–1093.

Forbes, G.S., and R.M. Wakimoto, 1983: A concentrated outbreak of tornadoes, downbursts and microbursts, and implications regarding vortex classification. *Mon. Wea. Rev.*, **111**, 220-235.

Fujita , T.T., 1978: Manual of downburst identification for project NIMROD. SMRP Research Paper 156, University of Chicago, 104 pp. [NTIS PB-28604801].

_______, 1981: Tornadoes and downbursts in the context of the generalized planetary scales. *J. Atmos. Sci.*, **38**, 1511-1534.

Przybylinski, R.W., 1995: The bow echo: Observations, numerical simulations, and severe weather detection methods. *Wea. Forecasting*, **10**, 203-218.

Trapp, R.J., and M.L. Weisman, 2003: Low-level mesovortices within squall lines and bow echoes. Part II: Their genesis and implications. *Mon. Wea. Rev.*, **131**, 2804-2823.

Weisman, M.L., 1993: The genesis of severe, long-lived bow echoes. *J. Atmos. Sci.*, **50**, 645-670.

_______, and R.J. Trapp, 2003: Low-level mesovortices within squall lines and bow echoes. Part I: Overview and sensitivity to environmental wind shear. *Mon. Wea. Rev.*, **131**, 2779-2803.